





The L4n laser beamline of the P3-installation: Towards high-repetition rate high-energy density physics at ELI-Beamlines

Cite as: Matter Radiat. Extremes 6, 015401 (2021); doi: 10.1063/5.0022120

Submitted: 17 July 2020 • Accepted: 24 October 2020 •

Published Online: 24 November 2020



N. Jourdain,¹ U. Chaulagain,¹  M. Havlík,¹ D. Kramer,¹ D. Kumar,¹  I. Majerová,¹  V. T. Tikhonchuk,^{1,2} 
C. Korn,¹ and S. Weber^{1,3,a)}

AFFILIATIONS

¹ELI-Beamlines, Institute of Physics, Czech Academy of Sciences, 18221 Prague, Czech Republic

²Centre Lasers Intenses et Applications, University of Bordeaux–CNRS–CEA, 33405 Talence, France

³School of Science, Xi'an Jiaotong University, Xi'an 710049, China

^{a)}Author to whom correspondence should be addressed: stefan.weber@eli-beams.eu

ABSTRACT

The P3 installation of ELI-Beamlines is conceived as an experimental platform for multiple high-repetition-rate laser beams spanning time scales from femtosecond via picosecond to nanosecond. The upcoming L4n laser beamline will provide shaped nanosecond pulses of up to 1.9 kJ at a maximum repetition rate of 1 shot/min. This beamline will provide unique possibilities for high-pressure, high-energy-density physics, warm dense matter, and laser–plasma interaction experiments. Owing to the high repetition rate, it will become possible to obtain considerable improvements in data statistics, in particular, for equation-of-state data sets. The nanosecond beam will be coupled with short sub-picosecond pulses, providing high-resolution diagnostic tools by either irradiating a backlighter target or driving a betatron setup to generate energetic electrons and hard X-rays.

© 2020 Author(s). All article content, except where otherwise noted, is licensed under a Creative Commons Attribution (CC BY) license (<http://creativecommons.org/licenses/by/4.0/>). <https://doi.org/10.1063/5.0022120>

I. INTRODUCTION

ELI-Beamlines is a part of the Extreme Light Infrastructure (ELI) project and will soon become one of the most powerful laser facilities in the world.^{1,2} Its experimental P3 platform for plasma physics is presented in Fig. 1. With the possibility of focusing in the interaction chamber up to four synchronized beams derived from the L3 (energy 30 J, pulse duration 30 fs, wavelength 800 nm, repetition rate 10 Hz) and L4 (1.9 kJ, 150 fs, 1053 nm) lasers with peak intensities of up to 10^{23} W/cm², experiments in a broad range of domains such as laser–plasma interaction, high-field physics, warm dense matter, high-energy-density physics, and plasma optics can be carried out on this installation.^{3–6} A detailed review of experiments to be performed on this plasma physics platform can be found in Ref. 7.

Of particular interest for the physics of matter in extreme states is the nanosecond high-energy L4n beam shown in pink in Fig. 1. The uniqueness of this kilojoule-class system relies on its ability to operate at a high repetition rate with the ultimate objective of providing up to 1 shot/min. This exclusive feature is of great interest for high-energy-density

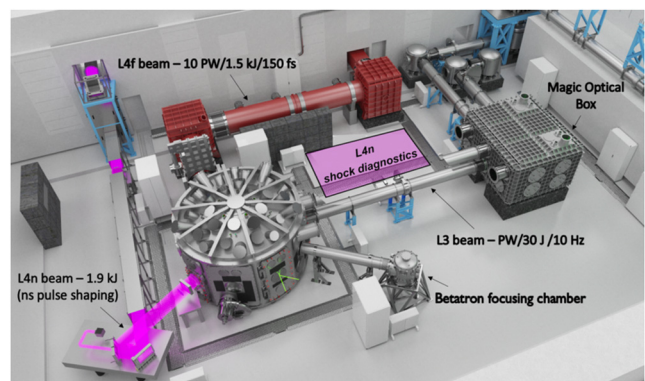


FIG. 1. The E3 experimental hall for plasma physics and beam configurations. The L4n pulse (1.9 kJ, 0.5 ns–10 ns, 1053 nm) is shown in pink. Three other beams will also be available in E3: L4f (1.5 kJ, 150 fs, 1053 nm), L4p (available in 2022) (150 J–400 J, 150 fs to 150 ps, 1053 nm), and L3 (30 J, 30 fs, 800 nm, 10 Hz).

TABLE I. Overview of the current performance of major high-energy laser facilities in a long-pulse configuration listing the name of the installation, the operating entity, the laser wavelength in nanometers, the maximum energy available per shot, and the operating repetition rate.⁷

Installation	Operating facility	λ (nm)	Maximum energy (long pulse)	Repetition rate
NIF	LLNL (Livermore, USA)	1053	2.1 MJ (3ω , 3 ns–15 ns)	Every 8 h
LMJ	CEA (Le Barp, France)	1053	1.4 MJ (3ω , 3 ns–15 ns)	Every 8 h
Omega EP	LLE (Rochester, USA)	1053	30 kJ (3ω , 1 ns–3 ns)	Every 90 min
SG-II-UP	SIOM (Shanghai, China)	1053	24 kJ (3ω , 3 ns)	Every 3 h
Gekko XII	ILE (Osaka, Japan)	1064	10 kJ (2ω , 1 ns)	Every 30 min
Orion	AWE (Aldermaston, UK)	1053	5 kJ (3ω , 1 ns)	Every 45 min
L4n	ELI-Beamlines (Prague, Czech Republic)	1053	1.2 kJ (2ω, 1 ns–5 ns)	1 shot/min
VULCAN	CLF, STFC (Oxford, UK)	1053	1 kJ (2ω , 1 ns–10 ns)	2 shots/day
PALS	IoP (Prague, Czech Republic)	1315	200 J (3ω , 250 ps)	Every 25 min
LULI 2000	LULI, CEA (Paris, France)	1053	750 J (2ω , 1.5 ns)	Every 90 min
MEC	SLAC (Menlo Park, USA)	1053	60 J (2ω , 10 ns)	Every 7 min
HIBEF	Eu-XFEL (Schenefeld, Germany)	1053	100 J (1ω , 10 ns)	10 Hz

physics experiments, since current high-energy facilities are generally limited to one or two shots per hour. The performances of several facilities in a long-pulse configuration and their repetition rates at full energy are listed in Table I.^{8–16} The biggest installations, namely, the National Ignition Facility (NIF) and the Laser Mégajoule (LMJ) facility, providing energies higher than 1 MJ and able to reach pressures of hundreds of gigabars,^{17–19} operate in single-shot mode. Facilities with kilojoule-class lasers offer users up to 2 shots/h, with achievable plasma pressures ranging from tens to hundreds of megabars.^{20,21} At the SLAC facility, the long-pulse system on the MEC platform can generate dynamically compressed matter to several megabars while probing it with bright X-ray free-electron laser (X-FEL) radiation.²² This will also soon be possible at the HED instrument of Eu-XFEL with the DiPOLE100X laser, expected to run at a considerably higher repetition rate of 10 Hz.²³ It follows clearly from Table I that L4n stands out from current kilojoule-class laser facilities with its dramatically higher repetition-rate capacity.

An increase in the shot number capacity will have a significant impact on fields related to inertial confinement fusion²⁴ and

laboratory astrophysics,²⁵ where experimental campaigns can span several years owing to limited access to laser infrastructures. In addition, modeling of matter under these extreme conditions can be very challenging because of strong correlations between particles compared with those in conventional plasmas. This considerably increases the need for robust experimental data.

Interpretations of data in high-energy-density physics experiments are not always straightforward and can lead to inconsistency among different studies. This applies in particular to dynamic compression experiments, which are affected by a shortage of statistics and large error bars. Major discrepancies were found in SiO₂ equation-of-state (EoS) measurements, which had a consequent impact on the determination of the deuterium EoS.²⁶ Accurate characterization of the properties of silica is crucial since it is extensively used in hydrodynamic simulations and in impedance matching measurements.²⁷ For this reason and many others, there is considerable interest among the scientific community in remedying the problem of a small database.

Two solutions have been envisaged to overcome this lack of statistics: either through obtaining more precise data by improving

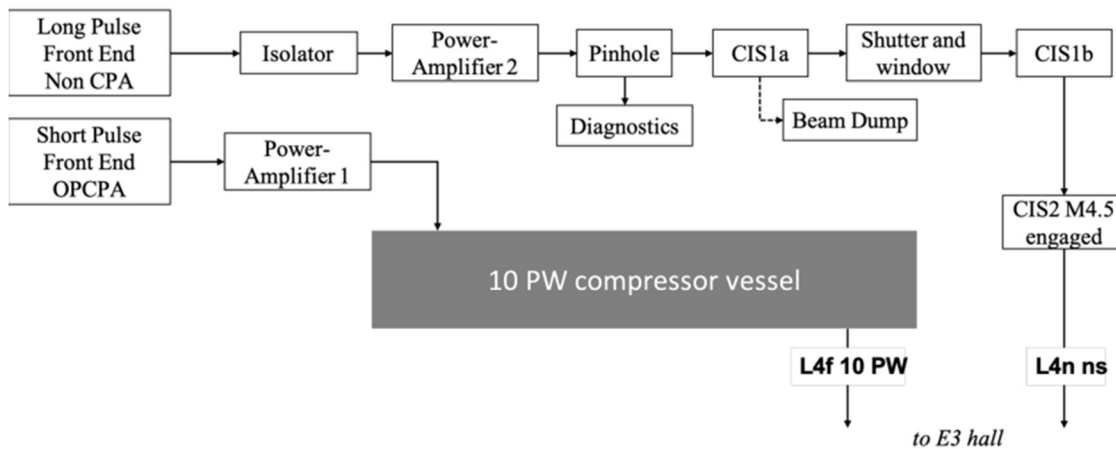


FIG. 2. Schematic of the L4 ATON laser in the high-power non-CPA configuration.

the measurement techniques and diagnostics or by significantly increasing the number of shots. While recent studies have proved that it is possible to acquire shock velocity measurements with uncertainties lower than 1%,²⁸ we present here an alternative solution with the L4n beamline, a long-pulse high-energy laser with unprecedented repetition-rate capacities. Improved diagnostics techniques will also be employed in the P3 installation.

The remainder of the paper is structured as follows. Section II describes the properties and layout of the L4n beamline together with the challenges arising from kilojoule-class laser operation at a high repetition rate. Section III deals with perspectives for future experiments, highlighting the specific contributions that L4n can provide for the study of matter in extreme states.

II. THE L4N BEAMLINE

A. L4 laser

The L4 laser will provide 10-PW-class peak power pulses, with nominal energy of 1.5 kJ and duration 150 fs. It is being developed by a consortium of the National Energetics/EKSPLA and ELI-Beamlines. An exhaustive description of the L4 laser is presented in Refs. 29–33. In addition to ultrashort pulses, the L4 laser architecture shown in Fig. 2 allows the generation of a nanosecond nonchirped pulse using a long-pulse narrowband front end connected directly to the final Nd:glass phosphate kilojoule amplifier. This amplifier employs face liquid cooling of the active medium, making it possible to fire a full-energy shot approximately every minute.

The compressor imaging system (CIS) is located in the hall adjacent to the E3 hall. Its final purpose is to transport the chirped beam from the laser to the compressor as well as the nonchirped beam to the L4n beamline on demand. The L4n pulse has to be diverted from the CIS path with a slide-in mirror. This is indicated as M4.5 in Fig. 2. During its passage through the CIS, the beam is magnified to its

TABLE II. L4n laser specifications.

Beam dimensions	$32 \times 32 \text{ cm}^2$
Central wavelength	$\lambda = 1053.2 \text{ nm}$
Energy	1.9 kJ
Pulse duration	$\tau = 0.1 \text{ ns} - 10 \text{ ns}$
Strehl ratio	~ 0.5
Pointing stability	$< 10 \mu\text{rad}$
Beam shape	Square super-Gaussian (order ~ 20)

final design aperture. The design of the CIS is shown in Fig. 3, where (a) is the baseline optical scheme for the chirped beamline and (b) is the layout for a long-pulse beamline with M4.5 mirror inserted up to the vacuum window in E3.

B. L4n beam properties

The main L4n pulse specifications are presented in Table II. The central input wavelength is $\lambda = 1053.2 \text{ nm}$ and can be converted to $\lambda_{2\omega} = 526.6 \text{ nm}$ with a frequency-doubling potassium dihydrogen phosphate (KDP) crystal. This scheme is conceived for the dynamic compression experiments. The use of a shorter wavelength allows a higher ablation pressure on the target, along with suppression of parasitic effects such as stimulated backscattering and production of hot electrons.

In addition, several conditions are required on the laser to enable the performance of high-energy-density physics experiments in a repetitive regime: the laser driver energy has to be reliable on a shot-to-shot basis, the intensity distribution over the focal spot should be as uniform as possible, and a very precise and reproducible pulse temporal profile is needed to control the pressure in the sample.

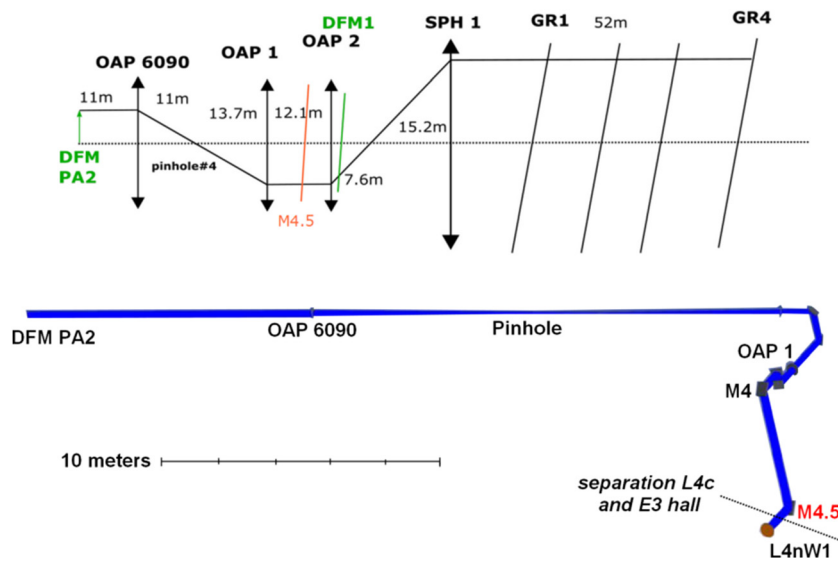


FIG. 3. Layout of the compressor imaging system (CIS) with its optical scheme in the chirped pulse beamline (a) and with the M4.5 mirror position defined from Zemax OpticStudio simulations (b).

C. Layout of beams in the E3 experimental hall

L4n experiments will be carried out in the E3 hall. The beamline design in this area is shown in Fig. 4. The separation between vacuum and air is made after the L4nW1 vacuum window at the entrance of the E3 hall. L4n is then brought to the target chamber center (TCC) level by two flat mirrors M1 and M2 held in a periscope tower. The beam is then converted into second harmonic with a KDP crystal and transported in air to the focusing system. This section of the beamline is protected with aluminum covers for safety reasons. Two dichroic mirrors M3 and M4 direct the beam to the P3 vacuum chamber and filter out the unconverted 1ω light. The energy contrast between the 1ω and 2ω components after reflections from the pair of dichroic mirrors is about 2.5×10^{-5} .

The L4n beam is then spatially smoothed with a phase plate. Currently, two distributed phase plates (DPPs) designed for focal spots with full width at half maximum (FWHM) of $500 \mu\text{m}$ and $700 \mu\text{m}$ are available. Initially, L4n will operate with a subaperture circular beam of 25 cm diameter imposed by the dimensions of the first set of KDP crystal and DPP available. The aspherical focusing lens with a back focal length of 2600 mm is located outside the P3 interaction chamber owing to concerns about debris. Particular attention is paid to ghost reflections, and the optical design has been realized accordingly. More details are provided in Sec. II D. Finally, the beam enters the vacuum chamber, passes through the debris shield, and is focused on the target. The debris shield is antireflection (AR)-coated for the wavelength of interest. Targets and most diagnostics will be located in the P3 vacuum chamber of diameter ~ 5 m, height ~ 3 m, and total volume $\sim 50 \text{ m}^3$. This

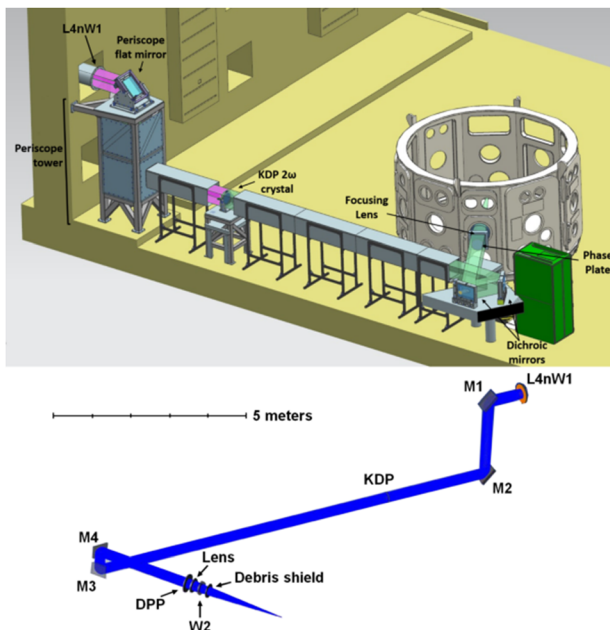


FIG. 4. (a) Design of the L4n beamline in the E3 experimental hall. The L4n beam is shown in pink up to the frequency-doubling KDP crystal. The converted 2ω beam is then shown in green. (b) Optical layout extracted from Zemax OpticStudio simulations.

TABLE III. Requirements on the nominal L4n design.

Requirement	Specification
Maximum energy 1ω	1.9 kJ
Maximum energy 2ω	1 kJ
Beam dimensions	25 cm diameter
initial phase	
Maximum energy 1ω subaperture beam	1 kJ
Conversion efficiency	Best effort >60%
Best spot diameter	$50 \mu\text{m}$
Spot diameter	$>300 \mu\text{m}$
after conditioning	
Nominal focus position	± 2 mm lateral/ ± 5 mm longitudinal
Synchronization	20 ps
Pointing stability	$<5 \mu\text{rad}$ on KDP crystal
Maximum repetition rate at 2ω	1 shot/min

massive experimental chamber provides opportunities for various setups with potentially a considerable number of diagnostics. The nominal requirements regarding L4n beamline performance are presented in Table III.

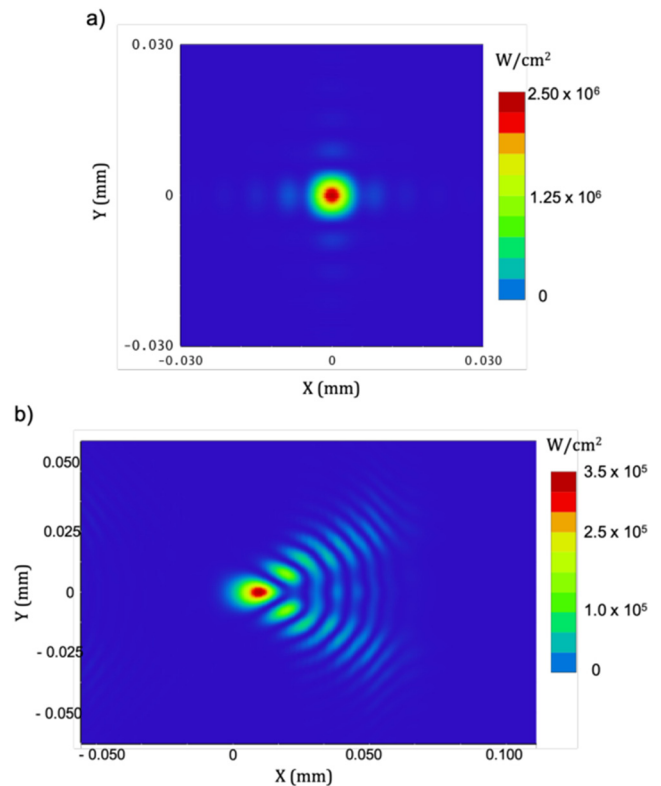


FIG. 5. (a) Diffraction-limited focal spot with 0.2° lens tilt and 1 W input power in a square beam. (b) Focal spot with 0.42° lens tilt and 1 W input power in a square beam.

TABLE IV. Main specifications of frequency-doubling KDP crystal.

Clear aperture	284 ± 1 mm
Phase matching angle	$59 \pm 0.2^\circ$
Damage threshold	>10 J/cm ² at 1 ns

D. Description of main L4n beamline optics

The beamline will be initially equipped with a subaperture round 300 mm KDP crystal, thus limiting the first-harmonic energy to 1 kJ. The remaining optical elements are being procured for the final square beam size as specified in Table II. The main focusing lens is located in air between the phase plate and vacuum window to avoid contamination or damage from the target debris. The positions of the ghost foci have to be strictly controlled to avoid damage to optical elements or plasma generation detrimental to the beam integrity.

The design process resulted in a meniscus lens with one aspherical side and a back focal length of 2600 mm. Only the conical constant was used for the departure from sphericity. The nominal focal spot diameter will be diffraction-limited if the phase plate is removed from the beamline, as shown in the OpticStudio simulation in Fig. 5(a). This is achieved despite the tilt of the lens and all the elements downstream. The primary ghost of the lens stays within the beam aperture but at a distance of 10 m, so that it cannot impact the 10 ns pulse. The remaining key ghost positions are located outside the beam path. Other ghosts have lower intensity than the primary beam. The lens can be tilted more if backpropagation is a problem during operation without KDP and the ghost beam has to be driven out of the beam aperture. The root-mean-square spot radius would still be acceptable with a FWHM of ~ 50 μm [see Fig. 5(b)], which is consistent with the requirements in Table III.

The L4n pulse will be frequency-doubled with a KDP crystal whose main specifications are listed in Table IV. The conversion efficiency simulated with the Miro model³⁴ is shown in Fig. 6 for a 1 kJ input corresponding to the maximum energy for the subaperture beam. Reflectivity and transmission losses are included in the calculation. For a 1 ns pulse duration, the conversion efficiency in the second harmonic is $\sim 80\%$ and drops to half of this value for a duration of 5 ns.

To achieve a uniform spatial pulse shape in the focal plane, two phase plates have been procured. These plates have continuously varying random phase profiles and are sol-gel AR-coated. The spot

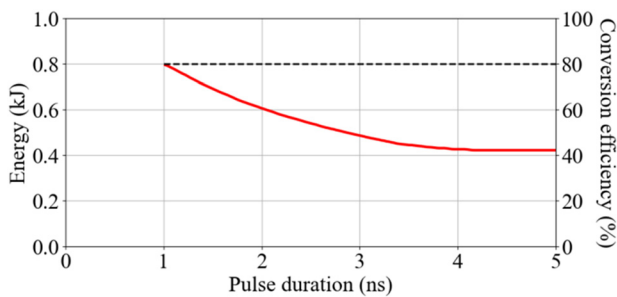


FIG. 6. Calculated KDP crystal conversion efficiency to second harmonic with 1 kJ as energy input.

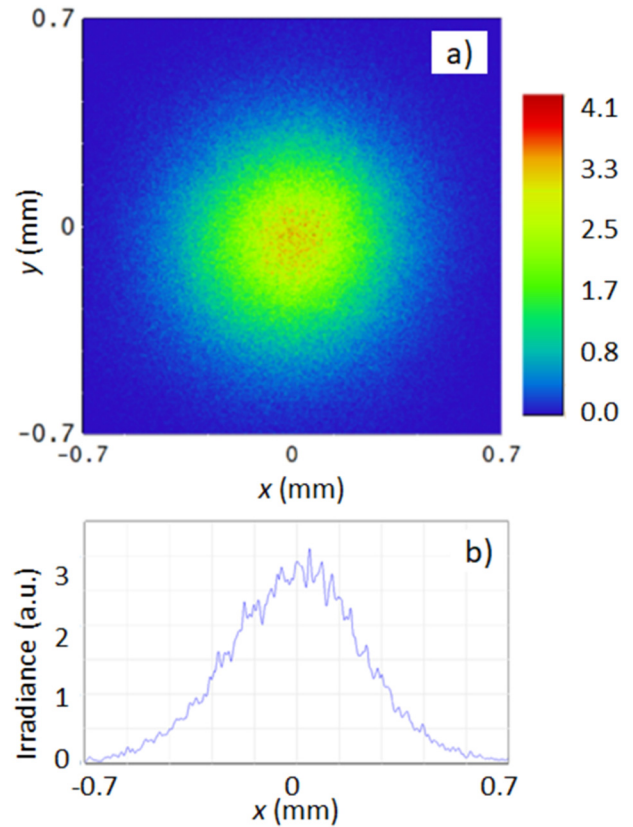


FIG. 7. (a) Focal spot intensity profile (arbitrary units) simulated using wave front data from one of the phase plates. (b) Horizontal slice of the intensity profile.

profile from a ray tracing simulation using the measured wave front data of the first wave plate is shown in Fig. 7. The second wave plate has a profile that is narrower by about 150 μm .

E. Repetition rate capacity

The repetition rate for the first experiment will be about one shot every 10 min. This rate is chosen as a compromise based on analysis of machine safety, the cooling rate of the conversion KDP crystal, and the wave front stability of the laser. Active cooling of the KDP crystal will be necessary in order to reach a higher repetition rate, since, according to our calculations, the conversion efficiency drops rapidly to 50% after several shots without cooling.

The actively cooled KDP system design is ongoing in parallel to the L4n beamline design and will be implemented soon after the initial experiments.

F. Beam diagnostics

The main laser diagnostics package will be located behind the second dichroic mirror. A spare lens from the main beamline will focus the leakage beam. The demagnified beam will be imaged to near-field diagnostics at the main wavelength and the second harmonic and far field at 2ω . The energy will be monitored for both harmonics as

well. The temporal pulse shape will be monitored by a high-bandwidth (11 GHz) transient digitizer with a high-precision timing reference. The amount of backreflection to the laser will be monitored for machine protection only if the KDP is not to be used.

G. Challenges with operation in a repetitive regime

High-energy lasers running at a considerable repetition rate face many challenges. The following are the main issues that have been foreseen.

First, the laser pulse quality needs to be good enough, with small shot-to-shot fluctuations. This means that the intensity distribution in the focal spot should be very stable and the temporal profile as robust as possible. This is crucial to increase the accuracy of the statistics in the datasets. Another major concern is related to targets. Mass production of targets is required, since hundreds of them will be shot per day.³⁵ The experimental platform should also ensure rapid positioning of targets within an accuracy of $\sim 50 \mu\text{m}$. Moreover, these targets produce a large amount of debris, about a few micrograms per shot, which can damage the optical elements. Thus, optical elements in the vacuum chamber have to be protected by a debris shield. The latter needs to be motorized so that it can be synchronized with the target displacements and not alter diagnostic signals. Target frames also have to be designed in such a way that debris from one target does not affect neighboring targets.

Appropriate vacuum conditions ($\sim 10^{-5}$ mbar) have to be maintained in the chamber throughout the shot sequences. Given the volume of the P3 interaction chamber ($\sim 50 \text{ m}^3$) and the substantial pumping system, this can be achieved without major difficulty. A big challenge is the need to collect and analyze large datasets. This requires high storage capability and the capability to perform on-line data analysis for rapid interventions during shots, if needed. Detectors also have to be compatible with multiple successive acquisitions while being remotely controlled. For example, image plates will no longer be appropriate for X-ray diagnostics, since they must be replaced after each shot, while the chamber cannot be vented between shots. Finally, protection from electromagnetic pulses (EMPs) must be ensured.^{36–38} This presents more threats for future multibeam experiments with the L4f, L4p, and L3 beams employing femtosecond pulses. These experiments will also bring the opportunity to perform direct EMP measurements. To mitigate the potential effects of EMPs at ELI-Beamlines, a mesh-grid-based earthing network is implemented. An EMP rack is available in the E3 hall for protection of electronic equipment.

III. PERSPECTIVES FOR FUTURE EXPERIMENTS

A. Pulse shaping to reach far-from-Hugoniot states

The use of steady shocks restricts studies to states along the Rankine–Hugoniot adiabat. To access states far from the Hugoniot, precise temporal shaping of the pulse is necessary. Various shock loading techniques like those described in Ref. 39 will be implemented in future L4n experiments. The temporal shaping resolution of an L4n pulse is ~ 150 ps. A steady shock will be considered in the first L4n commissioning experiment. If temporal pulse shaping is successful and leads to reproducible and well-controlled shocks, more complex pulse shapes will be used in future experiments.

Figure 8 presents several pulse temporal profiles and the corresponding states with respect to the Hugoniot adiabat in the P – ρ

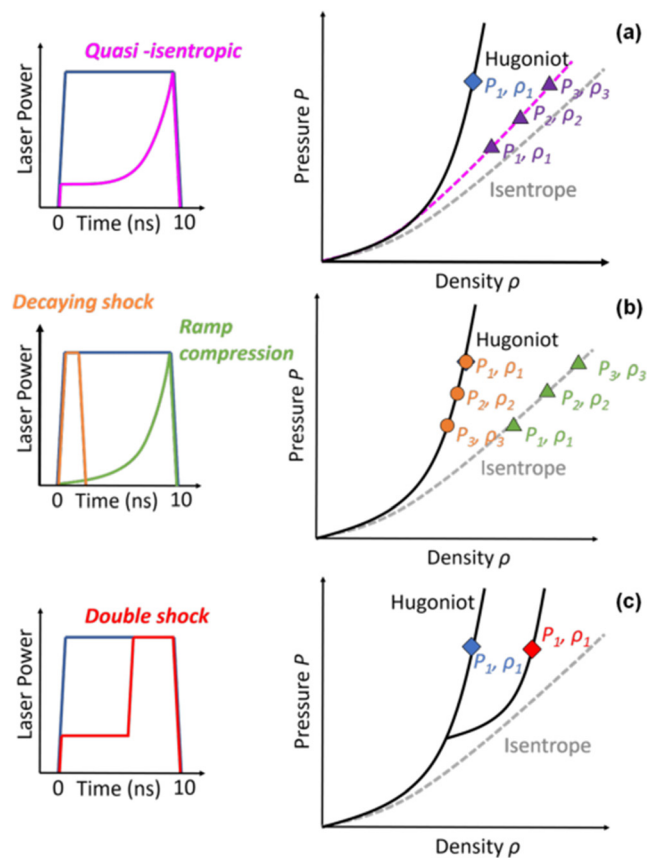


FIG. 8. The left panels show laser pulse temporal profiles providing access to the Hugoniot adiabat and far-from-Hugoniot states. The right panels show the corresponding trajectories in the phase plane P – ρ . (a) Steady and quasi-isentropic compression. (b) Decaying shock and ramp compression. (c) Double shock. Adapted from Refs. 39,40.

diagram. Aside from the steady compression [the solid line in Fig. 8(a)], decaying shocks allow one to access several points along the Hugoniot line [the solid line in Fig. 8(b)]. In the latter case, one can use a square pulse of short duration (~ 1 ns or less). One potential application of this scheme is to the study of phase transitions. The use of ramp compression [Fig. 8(b)], where the laser power gradually increases over the whole pulse duration, provides the opportunity to characterize states along the isentrope.

In addition, more sophisticated pulse shaping techniques can be used in dynamic compression experiments. This includes quasi-isentropic compression [Fig. 8(a)], where a first weak shock is followed by a ramp compression. The first weak shock brings matter to states located on a higher isentrope compared with regular ramp compression. This quasi-isentropic compression requires long pulses and a high-energy (>1 kJ) laser. Finally, a double shock or “dynamic precompression” [Fig. 8(c)] can provide access to states at lower temperatures than the Hugoniot adiabat, which is relevant to studies of planetary interiors.⁴¹ Accurate control of timing and the laser intensity profile is necessary, and moderate pulse energies of a few hundred joules are sufficient.

B. Demonstrating the benefit of the increase of statistics in EoS measurements

One of the major contributions of the L4n beamline to the scientific community will be an improvement in data interpretation by decreasing the statistical errors in experiments performed with kilojoule-class lasers. Such progress will be demonstrated under the experimental conditions that have allowed ambiguous interpretations in several works over the past years.

The element chosen for this study is magnesium oxide (MgO), which is of great importance for planetary science since it is a major component of the deep mantles of terrestrial planets and exoplanets. Despite numerous studies in recent years, the MgO phase diagram and the phase transition boundary conditions in the pressure–temperature (P – T) diagram at high pressure (up to ~ 7 Mbar) are still uncertain.^{42–45} Our experiment will provide a much larger amount of data, thus improving the statistics, allowing for discrimination between models, and providing an unambiguous interpretation.

The experimental data will be compared with theoretical models reported in Refs. 46, 47. While differences between theoretical predictions are as low as a few percent, experimental points have more than 10% uncertainty. That is why one of the main goals of our experiment will be to reproduce published data with the improved statistics. As a first step, the MgO EoS will be measured along the principal Hugoniot adiabat and compared with the existing experimental data from Ref. 48. In the next step, a technique of decaying shocks will be applied.⁴⁵ We will study the solid-to-liquid phase transition in MgO and the boundary between the B1 and B2 crystalline phases.

C. Multibeam experiments

In future experiments, the high-energy L4n pulse will be coupled with petawatt pulses produced by the L3 laser. Figure 9 presents two possible configurations in the P3 vacuum chamber, with the L4n pulse shown in green and the L3 pulse shown in yellow. In the long-focal-length configuration, the L3 beam will be used for generation of a hard X-ray pulse via betatron emission, and this will be directed to the TCC at an angle of 112° with respect to the L4n beam. In the short-focal-length configuration, the L3 beam will be directly focused to the TCC at an angle of 58° with respect to the L4n beam for diagnostic purposes.

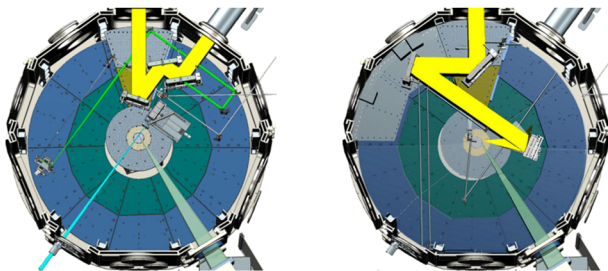


FIG. 9. Configurations for multibeam experiments with L4n (green) and L3 (yellow) pulses: (a) long-focal-length (5 m) configuration in which L3 is focused in a gas jet and generates relativistic electrons and broadband hard X-rays at an angle of 112° with respect to the L4n beam; (b) short-focal-length ($f = 750$ mm) configuration in which the L3 pulse is focused by an off-axis parabola (OAP) at an angle of 58° with respect to the L4n beam.

In the long-focal-length configuration, L3 is focused over 5 m by an $f/20$ spherical mirror in a gas jet and drives a relativistic electron beam via laser wakefield acceleration (LWFA). The complete experimental layout of this betatron setup on the P3 platform is described in Ref. 49. By using a laser pulse with an energy of 30 J and a duration of 30 fs, the electrons can be accelerated to energies in the range 400 MeV–1500 MeV with a total charge of up to 100 pC and a divergence of less than 10 mrad.⁵⁰ These accelerated electrons generate X-ray pulses via the betatron mechanism. The main features of the betatron X-ray source are a broadband spectrum (5 keV–100 keV), a high flux of $\sim 10^{11}$ photons/shot, a small source size (a few micrometers), a short pulse duration (< 10 fs), a narrow divergence (< 20 mrad), and an inherent synchronization with the driving pulse.⁵¹ This source provides a very high peak brightness, several orders of magnitude higher than conventional X-ray backlighter sources, because of its short pulse duration. The photon energy of the source and flux can be tuned by varying the laser energy and the gas jet design.⁵² In addition, owing to the micrometer-scale source size, this X-ray source possesses good spatial coherence, which also enables phase contrast imaging.⁵³ For applications requiring a focused X-ray beam, a broadband X-ray Kirkpatrick–Baez mirror⁵⁴ will be implemented in the interaction chamber.

In the short-focal-length configuration, the L3 pulse will be directly focused on the target with an $f/3$ off-axis parabola (OAP). This offers the possibility of generating hard X-rays^{55,56} or high-energy protons⁵⁷ from solid targets suitable for diagnostic purposes. While a single high-energy laser pulse is sufficient for producing X-rays and hot electrons in solid or compressed samples,^{58,59} supplementary laser beams are generally needed for probing dense materials. The following are examples of high-energy-density physics experiments to be performed on the P3 installation with L3 and L4p pulses in combination with an L4n high-energy pulse:

- Time-resolved pump–probe experiments can be performed in warm dense matter, with the L4n pulse acting as a pump beam. The broadband betatron X-ray beam will be used to perform time-resolved X-ray absorption studies.⁶⁰ With a high-flux betatron X-ray source, it is possible to obtain absorption spectra in a single shot.⁶¹ The ultrashort duration of betatron X-rays opens up the possibility of observing phenomena occurring on a femtosecond time scale.⁶² X-rays generated from backlighter solid targets are also suitable for such measurements,⁶³ and they can also be employed for X-ray Thomson scattering studies⁶⁴ or diffraction experiments using K_α X-ray narrowband emission.⁶⁵
- Bright and broadband betatron X-ray emission is an ideal source providing a real-time, nonintrusive diagnosis of material behavior at the micro- and mesoscales.⁶⁶ It can be used for imaging of strong shocks driven by the L4n laser. Shock wave propagation can also be monitored by phase contrast imaging⁶⁷ or radiography^{68,69} using X-rays from backlighter targets. Proton beams produced by the interaction of intense L3 and L4p laser pulses with solid targets can act as probes to characterize the electric and magnetic fields in plasmas produced by the L4n pulse.^{70,71}
- A nanosecond kilojoule L4n laser pulse can drive a hypersonic radiative shock wave in a gas target, which is relevant to astrophysical objects.^{72,73} The downstream plasma can be compressed beyond the critical density, and so commonly used optical plasma diagnostics cannot probe these structures. The X-ray backlighter

source^{74,75} and the betatron X-ray beam can provide a high-temporal-resolution and high-contrast image of fast-moving shock waves.

IV. CONCLUSIONS AND PERSPECTIVES

The L4n laser at ELI-Beamlines offers users a platform for high-energy-density physics experiments at a high repetition rate. This is of great interest in this field, where the available data suffer from poor statistics. The first, short-term, objective is commissioning of the L4n beamline and shock diagnostics in a dynamic compression experiment. Implementation of active cooling of the KDP conversion crystal will then allow the repetition rate to be increased to an unprecedented level of 1 shot/min. This platform for high-energy-density physics will subsequently be developed with complementary tools, including hard X-ray and high-energy charged particle diagnostics, which can provide key information about the structural evolution of materials under extreme pressures and temperatures.

ACKNOWLEDGMENTS

The authors acknowledge support from the projects “Advanced Research Using High Intensity Laser Produced Photons and Particles (ADONIS)” (Grant No. CZ.02.1.01/0.0/0.0/16_019/0000789) and “High Field Initiative (HiFI)” (Grant No. CZ.02.1.01/0.0/0.0/15_003/0000449), both from the European Regional Development Fund. The results of the Project LQ1606 were obtained with financial support from the Ministry of Education, Youth and Sports as part of targeted support from the National Program of Sustainability II.

REFERENCES

¹ELI Extreme Light Infrastructure (Whitebook), edited by G. Mourou, G. Korn, W. Sandner, and J. Collier (THOSS Media GmbH, Berlin, Germany, 2011).

²See <http://www.eli-beams.eu> for extreme light infrastructure beamlines.

³G. A. Mourou, T. Tajima, and S. V. Bulanov, “Optics in the relativistic regime,” *Rev. Mod. Phys.* **78**, 309 (2006).

⁴R. P. Drake, *High-Energy-Density Physics: Fundamentals, Inertial Fusion, and Experimental Astrophysics* (Springer Verlag Berlin, 2006).

⁵*Frontiers and Challenges in Warm Dense Matter*, edited by F. Graziani, M. Desjarlais, R. Redmer, and S. Trickey (Springer International Publisher, 2014).

⁶C. Thauray, F. Quéré, J.-P. Geindre *et al.*, “Plasma mirrors for ultrahigh-intensity optics,” *Nat. Phys.* **3**, 424 (2007).

⁷S. Weber, S. Bechet, S. Borneis *et al.*, “P3: An installation for high-energy density plasma physics and ultra-high intensity laser–matter interaction at ELI-Beamlines,” *Matter Radiat. Extremes* **2**, 149 (2017).

⁸E. I. Moses, R. N. Boyd, B. A. Remington *et al.*, “The national ignition facility: Ushering in a new age for high energy density science,” *Phys. Plasmas* **16**, 041006 (2009).

⁹J.-L. Miquel, C. Lion, and P. Vivini, “The laser mega-joule: LMJ & PETAL status and program overview,” *J. Phys.: Conf. Ser.* **688**, 012067 (2016).

¹⁰J. Kelly, L. Waxer, V. Bagnoud *et al.*, “OMEGA EP: High-energy petawatt capability for the OMEGA laser facility,” *J. Phys.* **133**, 75–80 (2005).

¹¹Y. Gao, W.-x. Ma, B.-Q. Zhu *et al.*, “Status of the SG-II-UP laser facility,” in *2013 IEEE Photonics Conference* (IEEE, 2013), pp. 73–74.

¹²N. Hopps, C. Danson, S. Duffield *et al.*, “Overview of laser systems for the Orion facility at the AWE,” *Appl. Opt.* **52**, 3597–3607 (2013).

¹³C. Danson, P. Brummitt, R. Clarke *et al.*, “Vulcan Petawatt—An ultra-high-intensity interaction facility,” *Nucl. Fusion* **44**, S239 (2004).

¹⁴K. Jungwirth, A. Cejnarova, L. Juha *et al.*, “The Prague asterix laser system,” *Phys. Plasmas* **8**, 2495–2501 (2001).

¹⁵M. Koenig, A. Benuzzi-Mounaix, N. Ozaki *et al.*, “High energy density physics on LULI2000 laser facility,” *AIP Conf. Proc.* **845**, 1421–1424 (2006).

¹⁶S. B. Brown, A. Hashim, A. Gleason *et al.*, “Shock drive capabilities of a 30-Joule laser at the matter in extreme conditions hutch of the linac coherent light source,” *Rev. Sci. Instrum.* **88**, 105113 (2017).

¹⁷O. Hurricane, D. Callahan, D. T. Casey *et al.*, “Inertially confined fusion plasmas dominated by alpha-particle self-heating,” *Nat. Phys.* **12**, 800 (2016).

¹⁸S. Le Pape, L. F. Berzak Hopkins, L. Divol *et al.*, “Fusion energy output greater than the kinetic energy of an imploding shell at the National Ignition Facility,” *Phys. Rev. Lett.* **120**, 245003 (2018).

¹⁹J.-L. Miquel and E. Prene, “LMJ and PETAL status and program overview,” *Nucl. Fusion* **59**, 032005 (2019).

²⁰S. Fujioka, Z. Zhang, N. Yamamoto *et al.*, “High-energy-density plasmas generation on GEKKO-LFEX laser facility for fast-ignition laser fusion studies and laboratory astrophysics,” *Plasma Phys. Controlled Fusion* **54**, 124042 (2012).

²¹A. Randewich and C. Danson, “High energy density physics at the atomic weapons establishment,” *High Power Laser Sci. Eng.* **2**, e40 (2014).

²²D. Kraus, J. Vorberger, A. Pak *et al.*, “Formation of diamonds in laser-compressed hydrocarbons at planetary interior conditions,” *Nat. Astron.* **1**, 606 (2017).

²³P. Mason, S. Banerjee, J. Smith *et al.*, “Development of a 100 J, 10 Hz laser for compression experiments at the high energy density instrument at the European XFEL,” *High Power Laser Sci. Eng.* **6**, e65 (2018).

²⁴R. Betti and O. A. Hurricane, “Inertial-confinement fusion with lasers,” *Nat. Phys.* **12**, 435 (2016).

²⁵B. A. Remington, “High energy density laboratory astrophysics,” *Plasma Phys. Controlled Fusion* **47**, A191 (2005).

²⁶M. D. Knudson and M. P. Desjarlais, “Shock compression of quartz to 1.6 TPa: Redefining a pressure standard,” *Phys. Rev. Lett.* **103**, 225501 (2009).

²⁷C. E. Ragan, “Ultrahigh-pressure shock-wave experiments,” *Phys. Rev. A* **21**, 458 (1980).

²⁸A. Fernandez-Pañella, M. Millot, D. E. Fratanduono *et al.*, “Shock compression of liquid deuterium up to 1 TPa,” *Phys. Rev. Lett.* **122**, 255702 (2019).

²⁹B. Rus, P. Bakule, D. Kramer *et al.*, “ELI-Beamlines: Development of next generation short-pulse laser systems,” *Proc. SPIE*. **9515**, 95150F (2015).

³⁰F. Batysta, R. Antipenkov, J. Bartonicek *et al.*, “Spectral shaping of a 5 Hz, multi-joule OPCPA frontend for a 10 PW laser system,” *Proc. SPIE*. **11034**, 11034OC (2019).

³¹S. Vyhlička, D. Kramer, M. Kepler *et al.*, “Optimization of a grating pulse stretcher suitable for kJ class 10 PW laser system,” *Proc. SPIE*. **10238**, 10238OT (2017).

³²G. Cheriaux, E. Gaul, R. Antipenkov *et al.*, “kJ-10 PW class laser system at 1 shot a minute,” *SPIE Proc.* **10898**, 1089806 (2019).

³³E. Gaul, G. Cheriaux, R. Antipenkov *et al.*, “Hybrid OPCPA/glass 10 PW laser at 1 shot a minute,” in *OSA Technical Digest (online)* (Optical Society of America, 2018), paper STu3M, STu3M.2.

³⁴O. Morice, “Miro: Complete modeling and software for pulse amplification and propagation in high-power laser systems,” *Opt. Eng.* **42**, 1530–1541 (2003).

³⁵I. Prencipe, J. Fuchs, S. Pascarelli *et al.*, “Targets for high repetition rate laser facilities: Needs, challenges and perspectives,” *High Power Laser Sci. Eng.* **5**, e17 (2017).

³⁶J. S. Pearlman and G. H. Dahlbacka, “Emission of rf radiation from laser-produced plasmas,” *J. Appl. Phys.* **49**, 457 (1978).

³⁷A. Poyé, S. Hulin, M. Bailly-Grandvaux *et al.*, “Physics of giant electromagnetic pulse generation in short-pulse laser experiments,” *Phys. Rev. E* **91**, 043106 (2015).

³⁸F. Consoli, R. De Angelis, T. Robinson *et al.*, “Generation of intense quasi-electrostatic fields due to deposition of particles accelerated by petawatt-range laser-matter interactions,” *Sci. Rep.* **9**, 8551 (2019).

³⁹T. S. Duffy and R. F. Smith, “Ultra-high pressure dynamic compression of geological materials,” *Front. Earth Sci.* **7**, 23 (2019).

⁴⁰R. Jeanloz, P. M. Celliers, G. W. Collins *et al.*, “Achieving high-density states through shock-wave loading of precompressed samples,” *Proc. Natl. Acad. Sci. U. S. A.* **104**, 9172 (2007).

- ⁴¹M. Guarguaglini, J.-A. Hernandez, A. Benuzzi-Mounaix *et al.*, “Characterizing equation of state and optical properties of dynamically pre-compressed materials,” *Phys. Plasmas* **26**, 042704 (2019).
- ⁴²R. S. McWilliams, D. K. Spaulding, J. H. Eggert *et al.*, “Phase transformations and metallization of magnesium oxide at high pressure and temperature,” *Science* **338**, 1330 (2012).
- ⁴³K. Miyanishi, Y. Tange, N. Ozaki *et al.*, “Laser-shock compression of magnesium oxide in the warm-dense-matter regime,” *Phys. Rev. E* **92**, 023103 (2015).
- ⁴⁴S. Root, L. Shulenburg, R. Lemke *et al.*, “Shock response and phase transitions of MgO at planetary impact conditions,” *Phys. Rev. Lett.* **115**, 198501 (2015).
- ⁴⁵R. M. Bolis, G. Morard, T. Vinci *et al.*, “Decaying shock studies of phase transitions in MgO-SiO₂ systems: Implications for the super-Earths’ interiors,” *Geophys. Res. Lett.* **43**, 9475 (2016).
- ⁴⁶R. Musella, S. Mazevet, and F. Guyot, “Physical properties of MgO at deep planetary conditions,” *Phys. Rev. B* **99**, 064110 (2019).
- ⁴⁷J. Bouchet, F. Bottin, V. Recoules *et al.*, “*Ab initio* calculations of the B1-B2 phase transition in MgO,” *Phys. Rev. B* **99**, 094113 (2019).
- ⁴⁸C. A. McCoy, M. C. Marshall, D. N. Polsin *et al.*, “Hugoniot, sound velocity, and shock temperature of MgO to 2300 GPa,” *Phys. Rev. B* **100**, 014106 (2019).
- ⁴⁹U. Chaulagain, K. Boháček, J. Vančura *et al.*, “LWFA-driven betatron source for plasma physics platform at ELI-Beamlines,” in *Proceedings of the 16th International Conference on X-Ray Lasers* (Springer Nature, Switzerland, 2020), p. 117, <https://doi.org/10.1007/978-3-030-35453-4>.
- ⁵⁰S. Fourmaux, E. Hallin, U. Chaulagain *et al.*, “Laser-based synchrotron x-ray radiation experimental scaling,” *Opt. Express* **28**, 3147 (2020).
- ⁵¹A. Rousse, K. T. Phuoc, R. Shah *et al.*, “Production of a keV x-ray beam from synchrotron radiation in relativistic laser-plasma interaction,” *Phys. Rev. Lett.* **93**, 135005 (2004).
- ⁵²M. Kozlova, I. Andriyash, J. Gautier *et al.*, “Hard x-rays from laser-wakefield accelerators in density tailored plasmas,” *Phys. Rev. X* **10**, 011061 (2020).
- ⁵³S. Fourmaux, E. Hallin, A. Krol *et al.*, “X-ray phase contrast imaging of spherical capsules,” *Opt. Express* **28**, 13978–13990 (2020).
- ⁵⁴P. Kirkpatrick and A. V. Baez, “Formation of optical images by x-rays,” *J. Opt. Soc. Am.* **38**, 766 (1948).
- ⁵⁵B. R. Maddox, H. S. Park, B. A. Remington *et al.*, “Absolute measurements of x-ray backlighter sources at energies above 10 keV,” *Phys. Plasmas* **18**, 056709 (2011).
- ⁵⁶M. Harmand, F. Dorchie, O. Peyrusse *et al.*, “Broad M-band multi-keV x-ray emission from plasmas created by short laser pulses,” *Phys. Plasmas* **16**, 063301 (2009).
- ⁵⁷K. Zeil, S. D. Kraft, S. Bock *et al.*, “The scaling of proton energies in ultrashort pulse laser plasma acceleration,” *New J. Phys.* **12**, 045015 (2010).
- ⁵⁸O. Renner, M. Šmíd, D. Batani, and L. Antonelli, “Suprathermal electron production in laser-irradiated Cu targets characterized by combined methods of x-ray imaging and spectroscopy,” *Plasma Phys. Controlled Fusion* **58**, 075007 (2016).
- ⁵⁹F. P. Condamine, E. Filippov, P. Angelo *et al.*, “High-resolution spectroscopic study of hot electron induced copper M-shell charge states emission from laser produced plasmas,” *High Energy Density Phys.* **32**, 89 (2019).
- ⁶⁰M. Z. Mo, Z. Chen, S. Fourmaux *et al.*, “Laser wakefield generated x-ray probe for femtosecond time-resolved measurements of ionization states of warm dense aluminum,” *Rev. Sci. Instrum.* **84**, 123106 (2013).
- ⁶¹B. Kettle, E. Gerstmayr, M. Streeter *et al.*, “Single-shot multi-keV x-ray absorption spectroscopy using an ultrashort laser-wakefield accelerator source,” *Phys. Rev. Lett.* **123**, 254801 (2019).
- ⁶²B. Mahieu, N. Jourdain, K. Ta Phuoc *et al.*, “Probing warm dense matter using femtosecond x-ray absorption spectroscopy with a laser-produced betatron source,” *Nat. Commun.* **9**, 3276 (2018).
- ⁶³A. Denoed, A. Benuzzi-Mounaix, A. Ravasio *et al.*, “Metallization of warm dense SiO₂ studied by XANES spectroscopy,” *Phys. Rev. Lett.* **113**, 116404 (2014).
- ⁶⁴K. Falk, S. P. Regan, J. Vorberger *et al.*, “Comparison between x-ray scattering and velocity-interferometry measurements from shocked liquid deuterium,” *Phys. Rev. E* **87**, 043112 (2013).
- ⁶⁵A. Denoed, N. Ozaki, A. Benuzzi-Mounaix *et al.*, “Dynamic x-ray diffraction observation of shocked solid iron up to 170 GPa,” *Proc. Natl. Acad. Sci. U. S. A.* **113**, 7745 (2016).
- ⁶⁶J. Wood, D. Chapman, K. Poder *et al.*, “Ultrafast imaging of laser driven shock waves using betatron x-rays from a laser wakefield accelerator,” *Sci. Rep.* **8**, 11010 (2018).
- ⁶⁷F. Barbato, S. Atzeni, D. Batani *et al.*, “Quantitative phase contrast imaging of a shock-wave with a laser-plasma based x-ray source,” *Sci. Rep.* **9**, 18805 (2019).
- ⁶⁸A. Ravasio, M. Koenig, S. Le Pape *et al.*, “Hard x-ray radiography for density measurement in shock compressed matter,” *Phys. Plasmas* **15**, 060701 (2008).
- ⁶⁹A. Morace, L. Fedeli, D. Batani *et al.*, “Development of x-ray radiography for high energy density physics,” *Phys. Plasmas* **21**, 102712 (2014).
- ⁷⁰R. A. Snavely, M. H. Key, S. P. Hatchett *et al.*, “Intense high-energy proton beams from Petawatt-laser irradiation of solids,” *Phys. Rev. Lett.* **85**, 2945 (2000).
- ⁷¹G. Sarri, C. A. Cecchetti, L. Romagnani *et al.*, “The application of laser-driven proton beams to the radiography of intense laser-hohlraum interactions,” *New J. Phys.* **12**, 045006 (2010).
- ⁷²R. P. Drake, F. W. Doss, R. G. McClarren *et al.*, “Radiative effects in radiative shocks in shock tubes,” *High Energy Density Phys.* **7**, 130 (2011).
- ⁷³P. Mabey, B. Albertazzi, E. Falize *et al.*, “Laboratory study of stationary accretion shock relevant to astrophysical systems,” *Sci. Rep.* **9**, 8157 (2019).
- ⁷⁴U. Chaulagain, C. Stehlé, J. Larour *et al.*, “Structure of a laser-driven radiative shock,” *High Energy Density Phys.* **17**, 106 (2015).
- ⁷⁵T. Clayson, F. Suzuki-Vidal, S. V. Lebedev *et al.*, “Counter-propagating radiative shock experiments on the Orion laser and the formation of radiative precursors,” *High Energy Density Phys.* **23**, 60 (2017).